Three-dimensional models of the cervicovaginal epithelia to study host-microbiome interactions and sexually transmitted infections

Vonetta L. Edwards[1,2], Elias McComb[1,†], Jason P. Gleghorn[3], Larry Forney[4], Patrik M. Bavoil[2,5] and Jacques Ravel[1,2]

[1] Institute for Genome Sciences, University of Maryland School of Medicine, Baltimore MD
[2] Department of Microbiology and Immunology, University of Maryland School of Medicine, Baltimore, MD
[3] Department of Biomedical Engineering, University of Delaware, Newark, DE
[4] Department of Biological Sciences, University of Idaho, Moscow, ID
[5] Department of Microbial Pathogenesis, Baltimore, MD
[†] Current address: University of Pennsylvania, Department of Obstetrics and Gynecology, Philadelphia, PA

Corresponding author:
Jacques Ravel: jravel@som.umaryland.edu
670 W. Baltimore Street
Baltimore, MD 21201

ABSTRACT Two-dimensional (2D) cell culture systems have provided controlled, reproducible means to analyze host-pathogen interactions. Although inexpensive, straightforward, and requiring very short time commitment, these models recapitulate neither the functionality of multi-layered cell types nor the microbial diversity of an infected human. Animal models have commonly been used to recreate the complexity of human infections. However, extensive modifications are commonly required to recreate interactions that resemble those in the human reproductive tract microbiologically and physiologically. Three-dimensional (3D) cell culture models have emerged as alternative means of reproducing key elements of human infections at a fraction of the cost of animal models and on a scale that allows for replicative experiments to be readily performed. Here we describe a new 3D model that utilizes transwells with epithelial cells seeded apically and a basolateral extra cellular matrix (ECM)-like layer containing collagen and fibroblasts. In this system, basal feeding creates a liquid/air interface on the apical side. The model produced tissues with close morphologic and physiological resemblance to human cervical and vaginal epithelia, including observable levels of mucus produced by cervical cells. Infection by both *Chlamydia trachomatis* and *Neisseria gonorrhoeae* was demonstrated as well as the growth of bacterial species observed in the human vaginal microbiota, enabling controlled mechanistic analyses of the interactions between host cells, vaginal microbiota and STI pathogens. Future experiments may include immune cells to mimic more closely the genital environment. Finally, the modular set up of the model makes it fully applicable to the analysis of non-genital host-microbiome-pathogen interactions.

IMPORTANCE Infected sites in humans are a complex mix of host and microbial cell types interacting with each other to perform specific and necessary functions. The ability to understand the mechanism(s) that facilitate these interactions, and interactions with external factors is paramount to being able to develop preventative therapies. Models that attempt to faithfully replicate the complexity of these interactions are time intensive, costly, and not conducive to high throughput analysis. Two-dimensional (2D) models that have been used as a platform to understand these interactions, while cost effective, are generally limiting in experimental flexibility and structural/physiological relevance. Our three-dimensional (3D) models of the cervicovaginal epithelium can facilitate analysis of interactions between the host epithelium, sexually transmitted pathogens and bacteria present in the vaginal microbiota. Due to the modular design, additional cell types and environmental modulators can be introduced to the system to provide added complexity, approaching conditions in the infected human host.

KEYWORDS: three-dimensional model, cervicovaginal epithelium, sexually transmitted infections, microbiome

Eukaryotic cell culture systems have been a staple of host-pathogenesis research for decades as they provide the means to model *in vivo* interactions in a controlled and reproducible *in vitro* environment. The mainstay of this approach is a flat surface 2-dimensional (2D) model where cells are grown as a monolayer on a solid impervious surface, usually plastic or glass treated with polymers that enhance cell adhesion. This method is inexpensive, accommodates many adherent cell types and imaging of the cells is relatively straightforward [1-3]. While 2D models have provided a wealth of information on host-pathogen interactions, they do not faithfully reproduce the physiological complexity of these interactions as they occur within or on the host organism. Notably, 2D cell culture systems may not be representative of *in vivo* cell morphology, lack true cellular junctional complexes and fail to account for the effect of differing cell types usually found within the environmental milieu [3, 4]. Experimentally, the design of the 2D systems is also limiting, as it does not allow the introduction of an air interface or the incorporation of extracellular matrices (ECM) that produce needed signaling and crosstalk molecules. This means that many of the predictions derived from 2D cell culture models do not hold true when applied to *in vivo* situations, as seen in cervical cancer models [5], and other pathogen-host models [6, 7].

To overcome these obstacles, models for multiple diseases and conditions have been developed in animals. These afford the ability to follow a progressing infection in a complex environment that can replicate many properties of the human host, e.g., local physiology and host response, but falls short on many others e.g., the structural and polymicrobial environments. Additional manipulations and modifications are also often required to maximize susceptibility to human-specific infectious agents [8-13]. The use of animal models for STI research is further complicated by the need to use animal-adapted pathogens strains, as is the case with *C. trachomatis*, or alternate species that have coevolved with their host, as is the case with *Chlamydia caviae* and *Chlamydia muridarium* [14-17]. Lastly, animal models are often expensive to develop and maintain. This high cost may limit the number of replicate experiments and thus exhaustive investigations are not usually undertaken.

Three-dimensional (3D) cell culture models provide a practical, cost-effective alternative to animal models while also greatly improving the modelling value of 2D culture systems. 3D models can capture many aspects of the native *in vivo* physiology including cell morphology, organization, and communication that cannot be replicated in typical 2D models. This includes, but is not limited to, the ability to replicate complex tissue interactions, create and maintain intercellular interactions including

junctional complexes, facilitate differentiation and polarization, mimic cellular behavior and integrate the site-specific microbial environment [4, 18-26]. Over the past decade various 3D cell culture reproductive tract model systems have been developed. These range from hydrogels [25, 27], and self-assembled organoids [3, 28], to microfluidics organ-on-a-chip models [23]. Hydrogels are usually placed on a scaffold and cells can be grown within or on top of the hydrogel, with 7 to 21 days necessary for full differentiation. These models have been used to analyze bacterial growth patterns, as well as targeted aspects of pathogenicity for multiple pathogens including ZIKA, HSV, *Chlamydia* spp., *Neisseria gonorrhoeae* and HIV [22, 29-34]. Similarly, self-assembled organoids can be grown either on a scaffold (i.e., collagen-coated beads) or scaffold free where cells are placed in suspension and self-aggregate to form a more complex structure. Organoid-based models have been used for mechanistic studies of bacterial pathogenesis [21, 28, 35-38]. 3D models generally closely mimic infections of multiple pathogens [22, 27, 30, 34, 36, 39] as well as environmental parameters [8, 29, 40] as they occur *in vivo*.

Whereas advances in hydrogel-based and organoid-based systems can recapitulate the 3D environment and multicellular nature needed to mimic aspects of the *in vivo* context, to an extent reproducibility is difficult owing to their stochastic cellular organization and/or time needed to establish the model. Organ on-a-chip models can overcome some of these limitations. Microfluidic modules that integrate parameters such as flow, mechanical stress, and the introduction of multiple environmental cues in any orientation around the cell(s) of interest can be developed [41-44]. This allows for organ-like systems that can be functionally maintained for extended periods of time allowing for more in-depth analysis. [20, 23]. However, the high cost of set up and maintenance of some of these models may not be feasible for many laboratories interested in studying host-pathogens interactions of the female reproductive tract. Indeed, there have been limited efforts towards the development of organ-on-a-chip systems to model infections of the reproductive tract.

In this study, we developed and characterized a 3D transwell cell culture model characterized by morphologically and physiologically differentiated vaginal and cervical epithelial cells that support the growth of bacteria found in the vaginal milieu and enable infection by both *C. trachomatis* [45] and *N. gonorrhoeae*. The transwell polyester membrane provides scaffolding support for the epithelial cells while allowing close proximity to an ECM and fibroblast network. By using the non-cancerous, mucin producing cell line (A2EN) [46], the model recapitulates critical aspects of the *in vivo* environment where mucins play an important role [47, 48]. Relatively low cost and short set-up time required to establish the model, enables the testing of multiple replicates in parallel under multiple conditions in a

120 semi-high throughput process. This model may serve as a primer for the future development of more
121 elaborate 3D organ-on-a-chip model systems.
122
123 **RESULTS**
124 **The epithelial 3D transwell model structurally resembles *in vivo* cervical and vaginal**
125 **epithelium**. Transwells, basally coated with collagen and in the presence of human fibroblasts,
126 mimicking the *in vivo* basement membrane of the epithelium, were used to develop a 3D model of the
127 female reproductive tract epithelia (Fig. 1). In these models, basal only feeding and air interface
128 exposure afforded the establishment of vaginal and cervical epithelia that morphologically closely
129 resemble the structure of these epithelia *in vivo* (Figs. 2 and 3). Polarization of epithelial cells over
130 time is usually an indication of their stage of development. We initially tested multiple types of
131 collagen and coating methods to determine optimal conditions. Epithelial barrier integrity was
132 evaluated using TEER values [49] measured over culture as the epithelial tissue formed. Basal
133 collagen coating and fibroblast embedding showed a gradual increase in TEER values with peaks of
134 approximately 600 ohms/cm^2 on day 6 for A2EN cervical epithelial cells (Fig. 2A) and 1000 ohms/cm^2
135 on day 8 for VK2 vaginal epithelial cells (Fig. 3A). Other methods of collagen coating and fibroblast
136 embedding, including apical coating (Figs. 2A and 3A), as well as basal or apical coating with
137 embedded fibroblasts were tested (data not shown). Embedding of fibroblasts was detrimental to the
138 integrity of the collagen layer and caused delamination from the transwell membrane.
139 Histology and electron microscopy were used to evaluate the structural and morphological
140 features of the two epithelial cells models. Hematoxylin and eosin (H&E) staining confirmed the
141 increased cell density and polarization of A2EN cervical epithelial cells (Fig. 2B) on day 6 as
142 compared to day 1. Morphologically, the epithelial structure was similar to that observed in
143 histological images of cervical tissue which comprises a compact single layer of epithelial cells (Fig.
144 2B). Transmission electron microscopy (TEM) further confirmed these observations. The A2EN
145 cervical epithelial cells form a monolayer of cells in tight contact with each other. An intact nucleus
146 and cilia on the surface of the cell were also observed (Fig. 2C).
147 An important feature of cervical cells is their ability to produce mucus [50, 51]. A2EN cervical
148 epithelial cells were selected for their demonstrated ability to produce mucus in a 2D model; a unique
149 and important feature of this cell line [46]. Immunostaining for mucin 5B, a major protein component
150 of mucus, shows that mucus is produced over a significant portion of the apical surface of the A2EN
151 cervical epithelium (Fig. 2D), thus recapitulating a critical functional property of the cervical
152 epithelium [51].

Histology and electron microscopy imaging of the VK2 vaginal epithelial model revealed a pronounced stratification at day 8 as compared to day 1 with multiple layers (up to 7) of cells observed (Fig. 3B and 3C). Further, maturation of VK2 epithelial cells was observed, with more mature cells in the upper layers and more immature cells in the lower layers. This organization mimics an integral feature of the vaginal epithelium, as glycogen, a key metabolite supporting the growth of the vaginal microbiota, accumulates in mature epithelial cells [52].

3D cervical A2EN cells are infected by *Chlamydia trachomatis* and *Neisseria gonorrhoeae*. The ability of *C. trachomatis* (Ct) serovar L2 to infect cervical A2EN cells was assessed in both a conventional 2D model (Fig. 4A) of cells grown on coverslips and in the 3D transwell model described herein (Fig. 4B). While both models facilitated relatively robust infectivity (Fig. 4C), the A2EN cervical epithelium 3D model accommodated higher infection (71%) compared to the 2D model (57%) (p-value 0.019). Both models were both infected with $2x10^5$ *C. trachomatis* elementary bodies representing a MOI of 2 and 1 for the 2D and 3D models respectively. Since the MOI was lower for the A2EN cervical epithelium 3D model, it demonstrated that a more efficient infection can be achieved in that model. The VK2 vaginal epithelium 3D model was also successfully infected with *C. trachomatis* (data not shown); however, as expected the level of infectivity was low (25%) since *C. trachomatis* predominantly infects cervical epithelial cells. TEM confirmed the infection, visualizing inclusions containing *C. trachomatis* at various developmental stages (Fig. 4D), with both elementary bodies (EBs) (infectious particles) and reticulate bodies (RBs) (metabolic/replicating particles) observed. While A2EN cervical epithelial cells are not robust producers of cytokines [46], we investigated the profiles of some common cytokines and found appreciable levels of IL-6, IL-8, IP10 and RANTES (Fig. 4E). These results are similar to those observed in Buckner et al [46], where perceptible levels of IL-6, IL-8, IP10 and RANTES were detected. We observed that the cytokine response of the model in the presence or absence of a chlamydial infection was similar to that previously observed in this and other human and mouse cell lines [53-56]. These results indicate that the A2EN cervical epithelium 3D model could serve as a suitable platform for studies of chlamydial infection.

Another common sexually transmitted pathogen is *N. gonorrhoeae* [57], with anecdotal evidence suggesting that *N. gonorrhoeae* infection might lead to an increased risk of *C. trachomatis* infection [58, 59]. Utilizing wildtype and mutants of a common *N. gonorrhoeae* laboratory-adapted strain FA1090, we showed that transmigration of *N. gonorrhoeae* takes place within 6 hours in the 3D cervical A2EN model. This is similar to the transmigration period observed with a HEC-1-B 3D cell model (Fig. 5A), a cell line commonly used to analyze *N. gonorrhoeae* infections [60-63]. TEM

imaging shows *N. gonorrhoeae* attached to the surface of the A2EN cells (Fig. 5B), which is the first step in the pathogenic cycle. These results suggest that the 3D A2EN cervical epithelium model can also support investigations of *N. gonorrhoeae* pathogenesis.

The 3D vaginal model can sustain the growth of vaginal bacteria. The vaginal microbiota plays a key role in the cervicovaginal microenvironment [64]. We developed conditions that afford the growth of *Lactobacillus crispatus* and *Gardnerella vaginalis* on the 3D vaginal epithelium model. These two species are prominent members of vaginal bacterial communities that are found in optimal and non-optimal conditions, respectively [65]. These bacteria were used to inoculate on the 3D vaginal epithelium model and shown to grow for at least 48h under anaerobic conditions. Growth was first demonstrated by measuring the pH of culture medium in the apical compartment after 48h of growth. Media containing *L. crispatus* had a significantly lower pH of ~4.2 as compared to *G. vaginalis* (pH 6.0) (Fig. 6A), As expected, *L. crispatus* acidified the microenvironment, while *G. vaginalis* did not. *In vivo* acidification is driven by the production of lactic acid by *L. crispatus,* typified with a higher proportion of D(-) lactate as compared to L(+) lactate [66-68]. A concentration of 7.41mM D(-) lactic acid was observed after 48h of growth with *L. crispatus* compared to 2.42 mM and 2.04mM with *G. vaginalis* or a no bacteria control, respectively **(**Fig. 6B**)**. This finding demonstrates that *L. crispatus* is metabolically active and growing on the 3D vaginal epithelium model. Further microscopic analyses using both TEM (Fig. 6C i, ii, iii) and FISH (Fig. 6C iv, v, vi) showed the presence of live *L. crispatus* **(**Fig. 6C ii, v**)** and *G. vaginalis* **(**Fig. 6C iii, vi**)** on the model under anaerobic conditions after 48h growth. It is important to note that the model was gently rinsed with PBS before fixation thus any non-adherent bacteria were removed, only bacteria attached to the epithelial surface or embedded in the mucin matrix were imaged. TEM afforded visualizing the physical localization of the bacteria in close proximity to the epithelial layer, while FISH staining confirmed the robust growth of the bacteria on the model. Viability staining **(**Fig. 6C vii, viii, ix**)** after 48h of bacterial growth indicated that vaginal epithelial cells remained viable (green staining on Fig. 6C), in contrast to a control comprising of epithelial cells exposed to 1% saponin which predominantly stain red and indicate dead cells **(**Fig. 6C x**)**.

DISCUSSION

2D cell culture models have been extensively used to study host-STI pathogen interactions. However, these models lack complexity and do not accurately mimic many of the physiological interactions that occur in host organisms, limiting interpretation and translation to complex human physiology. More specifically, 2D culture models are unable to recapitulate the native microenvironment including multicellularity, the composition of extracellular matrices (ECM), or various physicochemical properties and spatiotemporal molecular gradients [4, 69]. As such, many of the predictions derived using these 2D cell culture models often do not hold true when applied to conditions *in vivo*, as seen in cervical cancer models [5] and other pathogen-host models [6, 70]. We have advanced these models by developing 3D organotypic models of cervical and vaginal epithelia that include an interstitial compartment of collagen and associated fibroblasts. 3D epithelial models provide enhanced morphological and physiological cellular structures that can include inter-cellular interactions (i.e., junctional complexes), complex tissue interactions, differentiated and polarized epithelial structures, which taken together better mimic *in vivo* cellular behavior [4, 18-23, 25, 28]. The multi-layered structure of these models affords increases in complexity and experimental flexibility, such as the potential addition of different cell types, or even immune cells. 3D cell culture models partly fill a gap between the cost effectiveness of 2D cell culture and the complexity and high cost of organoids, organ-on-a-chip systems or animal models [8, 9, 11-13]. Animal models can be of limited use to study host-STI pathogen interactions because they are often lacking anatomical similarity to the human vaginal epithelium. For example, the lower reproductive tract of the mouse, an animal model commonly used in STI research, comprises of a keratinized stratified epithelium, while that of human is not keratinized. The 3D organotypic model we have developed is ideally suited for studies on the pathogenesis of STIs as it replicates many features of human cervicovaginal epithelia without the complexity, experiment-to-experiment variability and/or cost of organoids and animals. This proposed model will ultimately provide a way to study how the cervicovaginal microbiota interact with the host, and how these interactions increase or reduce the risk of infections by sexually transmitted pathogens.

We have shown that the model supports infection by *C. trachomatis* and *N. gonorrhoeae*, two of the most prevalent infections worldwide. *C. trachomatis* is an obligate human pathogen that requires host internalization for propagation while *N. gonorrhoeae* can replicate both outside and inside of epithelial cells. The 3D cervical model was able to reproduce characteristic features of infection by both pathogens. One can envision using these models to study co-infections or the role of a primary infection by *C. trachomatis* in susceptibility to infection by *N. gonorrhoeae,* or vice versa. Other potential co-infections, including with HSV, HPV or HIV could also be investigated. The model can be

enhanced further by adding more complex structures such as endothelial and/or immune cells to the basal compartment.

Importantly, the ability to grow vaginal bacteria on the 3D models of the vaginal and cervical epithelia is a critical first step toward modeling the *in vivo* complex microenvironment that includes a functional microbiota. Little is known about how the vaginal microbiota contributes to modulating the risk to STIs. Previous studies have postulated that indole-producing bacterial species such as *Prevotella, Petpostreptococcus* or *Peptinophilus* spp. can facilitate *C. trachomatis* replication [71-73], since *C. trachomatis* can use indole to synthesize tryptophan, an essential amino acid that genital *C. trachomatis* strains are incapable of producing. Tryptophan is present in the host extracellular and cytoplasmic compartments but can be depleted through the action of interferon (IFN)-γ which induces tryptophan catabolism by indoleamine-2,3-dioxygenase I (IDO) [74]. Mechanisms such as this have been difficult to study for at least three reasons: (1) it is unethical to perform many of these experiments in humans; (2) there are no cellular or biomimetic models of the cervicovaginal environment that include the microbiota; and (3) key features of the cervicovaginal space such as the dominance of *Lactobacillus* spp. and a low environmental pH (<4.5) are not found in other mammals that might otherwise be candidate animal models [75-77]. The 3D models developed in this study represent the first steps toward more advanced models that include complex microbiota. This component is critical, as the cervicovaginal microbiota exists in a mutualistic relationship with the cervicovaginal epithelium and is believed to play an important role in the risk to STIs. The microbiota is thought to constitute the first line of defense against STIs, but the mechanism(s) by which it exerts its protective effect(s) is/are unknown. Access to a model that reproduces the physiology and microbiology of the cervicovaginal space is thus critical. We have previously shown that an optimal microbiota dominated by *Lactobacillus* species, such as *L. crispatus*, produces copious amounts of lactic acid and a concomitant low environmental pH (<4.5). Lactic acid does not directly affect *C. trachomatis* bacteria but acts on the epithelium by decreasing epithelial cell proliferation, thus significantly inhibiting the infection process [45]. On the other hand, microbiota compositions associated with an increased risk to STIs tend to be similar to those observed in association with bacterial vaginosis (BV). BV is a condition that is generally defined by a high pH (>4.5), a microbiota characterized by the absence of *Lactobacillus* spp. and the presence of an array of strict and facultative anaerobes such as *G. vaginalis, Atopobium vaginae,* and *Prevotella* spp. The mechanisms by which a STI-permissive microbiota increase the risk to infection remains poorly understood. Based on our previous research we posit that a non-permissive indigenous microbiota interacts with the cervicovaginal epithelium to establish a homeostatic state that blocks STI and/or reduces disease

severity. Conversely, we propose that a permissive microbiota disrupts host epithelial cell homeostasis, thereby allowing STI to progress. Establishing reconstituted STI-permissive or non-permissive microbiota on an advanced 3D epithelial models will go a long way toward testing these hypotheses and improving our knowledge of the pathogenesis of STIs.

The 3D models developed in this study uses relatively inexpensive materials compared to organoids or organ-on-a-chip systems. These low-cost models afford performing replicate experiments in a semi high-throughput setup. In addition, this 3D model allows performing different analyses from one or replicate transwells, including resistance readings, measurements of pH, metabolite concentrations (i.e., lactate), cytokine concentrations, bacterial enumeration, and imaging (fluorescence, TEM) or omic analysis (DNA/RNA sequencing, proteomics, among others). Lastly, while we developed this system with A2EN cervical and VK2 vaginal cell lines, there is no barrier to using different cell lines more appropriate to the research questions at stake, or even from different organ systems or tissues.

MATERIALS AND METHODS

Abbreviations and all catalog numbers are listed in the supplemental materials.

Cell Culture Model: collagen coating. Transwell inserts (Corning #3472) were removed from the 24-well plate using glass pipettes or tweezers and placed in an inverted orientation into 12-well plates. To form the collagen coating, all solutions were chilled and placed on ice. 200µl 5X RPMI (1:1 mixture of 10X RPMI and tissue culture (TC) water) (Sigma #R1145) and 25µl 1M NaOH (Sigma #S5881) were combined and vortexed thoroughly for 10 secs. Rat tail collagen (800µl; Corning #354236) was added with gentle pipetting to avoid introducing excessive bubbles, and the pH of the mixture was tested. Additional NaOH or RPMI was added in 1µl or 10µl increments if needed to attain a pH of 6.5 (the final mixture should have a salmon pink color). A total of 70µl of the collagen mixture was added to the basal surface of each transwell insert, the plate was covered ensuring no contact with the collagen surface and the collagen allowed to gel in a Biosafety Level 2 (BSL2) hood at room temperature for ~30 min. (Fig. 1A). Using clean glass pipettes or tweezers the inserts were returned to the 24-well plate in the standard orientation and left under the hood for an additional 3h before transfer to 4°C for 48-72h.

Cell Culture Model: addition of fibroblasts. After 48-72h, the transwells were inverted into a 12-well plate using glass pipettes or tweezers. BJ fibroblast cells (ATCC #CRL 2522) at 70-90% confluency after growth in BJ complete medium (DMEM media (Cellgro #15-013-CV) supplemented with 10% FBS (Sigma #F4135)) were trypsinized using 1ml of 0.25% Trypsin (Gibco #25200-056)

and cell number determined using the Countess Automated Cell Counter. A total of $3x10^4$ cells in a volume of 75-80µl were added to the basal surface of the transwells on top of the collagen (Fig. 1B). The dish was covered and placed in a 37°C, 5% CO_2 incubator for 6h. Inserts were then transferred to the 24-well plate in the standard orientation and BJ complete medium added (200µl to the apical compartment, 500µl to the basal compartment). The transwells were then returned to the incubator for an additional ~42h.

Cell Culture Model: addition of epithelial cells. Either A2EN cervical epithelial cells (kindly provided by Dr. Allison Quayle [46]) or VK2/E6/E7 vaginal epithelial cells (ATCC #CRL 2616) were used to make cervical or vaginal models respectively. A2EN cervical cells were grown in A2EN complete medium (EpiLife media (Gibco #MEPICFPRF) with 100X EDGS supplement (Gibco #S-012-5) and 100X L-glutamine (Lonza #17-605E)) while VK2/E6/E7 vaginal cells (ATCC #CRL 2616) grown in VK2 complete medium (Keratinoctye-SFM (with BPE and EGF) (Gibco #10725-018) supplemented with 0.4M calcium chloride (Amresco #E506) and 100X L-glutamine (Lonza #17-605E)). Cells were grown until 70-90% confluent then trypsinized using 1ml of 0.25% Trypsin. The number of cells was determined using the Countess Automated Cell Counter. BJ complete medium was removed from the transwells which were then gently rinsed with 500µl PBS. To seed the epithelial cell layer, using A2EN or VK2 complete medium (cervical and vaginal model respectively) a total of $1x10^5$ epithelial cells in 200 µl of media was added to the apical compartment and 500 µl of media was added to the basal compartment and the plate returned to the incubator. After 48h the apical and basal media were removed by vacuum aspiration and fresh medium added to the basal compartment only, to create an epithelial- air interface. Fresh medium (500µl) was added to the basal compartment every other day. Following culture A2EN: 6 days and VK2: 8 days epithelial cells were polarized and no medium could be observed entering the apical compartment from the basal compartment, indicating stable epithelial barrier formation.

***Chlamydia trachomatis* infection, microscopy imaging and cytokine analysis.** *C. trachomatis* serovar L2 (strain LGV/434/Bu) was propagated in HeLa monolayers as previously described in Tan *et al.* [78]. Briefly, serovar L2 was cultivated in $100mm^2$ tissue culture dishes containing HeLa cells grown at 37°C, 5% CO_2. Monolayers were gently rocked for 2h, fresh medium was added, and the infection was allowed to progress for 48h. Lysates were harvested, and inclusion-forming units (IFUs) calculated and stored in sucrose phosphate glutamate (SPG) [78] at -80°C. Seeds were used directly from -80°C stocks. *C. trachomatis* was inoculated at a multiplicity of infection (MOI) of 1 or 2.

348 The 3D model was inoculated with 50µl *C. trachomatis* in the apical compartment and rocked
349 for 2h at room temperature. The *C. trachomatis* suspension was removed by pipetting, the cells were
350 rinsed with 500µl PBS, fresh medium (500µl) added basally, and the model was incubated for an
351 additional 46h at 37°C, 5% CO_2.
352 Following infection, the transwells were prepped for imaging as described in the fluorescence
353 staining section and images were obtained using a Zeiss Duo 5 confocal microscope and 3 consecutive
354 Z stack slices were compressed to create images for confocal analysis. For electronic microscopy, the
355 transwells were placed in glutaraldehyde fixative for processing and imaged on the Tecnai T12
356 Transmission Electron microscope. For comparative purposes A2EN cells were grown on coverslips
357 (2D) for 2 days and then infected with *C. trachomatis* at MOI 2 [79]. Infection and staining were
358 performed as described below with images obtained using a Zeiss Axio Imager Z1 (Zeiss). Infected
359 cells were manually identified using the ImageJ software (NIH).
360 For cytokine analysis, medium was removed from the basal compartment and stored at -80°C.
361 Seven cytokines: EGF, IL-6, IL-8, IP10, MDC, PDGF-AA and RANTES were analyzed using a
362 Luminex Multianalyte assay at the UMB Cytokine Core Laboratory.
363 ***Neisseria gonorrhoeae* infection and analysis.** 3D models containing $2x10^5$ A2EN cells was
364 exposed apically to 100µl of *N. gonorrhoeae* FA1090 wildtype or *N. gonorrhoeae* Opaless (all *opa*
365 genes deleted) or *N. gonorrhoeae* Δ*pilE*Δ*opa* (*pilE* and all *opa* genes deleted) at MOI of 10 for 6h at
366 37°C, 5% CO_2. The basal medium (500µl) was then removed and dilutions were plated on GCK agar
367 plates to determine the number of *N. gonorrhoeae* bacteria that transmigrated within the 6h incubation
368 period. For comparison $2x10^5$ HEC-1-B endometrial cells utilizing the same 3D set-up were exposed in
369 parallel and the transmigrated *N. gonorrhoeae* bacteria were quantified.
370 **Bacterial growth (*L. crispatus, G. vaginalis*) and microscopy imaging.** The optical densities
371 (OD) of bacterial cultures grown overnight in their respective media (*L. crispatus* in NYCIII and *G.*
372 *vaginalis* in TSB+5% horse serum) were determined using an OD to colony forming units (CFU)
373 conversion of 1 OD represents $1x10^9$ CFU. A volume corresponding to $2x10^8$ CFUs was added to the
374 experiment culture medium (a 2:1 mixture of complete cell culture medium: bacteria culture medium)
375 to produce a final volume of 1ml. A 10-fold dilution was then performed using experiment culture
376 medium and 100µl was added to the apical compartment of the model ($1x10^6$ CFU). Cells exposed to
377 bacteria or medium only (no bacteria control) were incubated for 48h under anaerobic conditions in a
378 37°C incubator within a Coy chamber. Aliquots of media were removed from the apical compartment
379 and the pH determined using an Apera Instruments PH8500 portable pH meter. Aliquots of 50µl were

used to determine the D(-) and L(+) lactic acid concentrations using the Boehringer Mannheim/R-Biopharm D-Lactic acid/L-Lactic acid kit as per manufacturer's instructions. Cells were gently rinsed with PBS and either fixed in 2.5% glutaraldehyde (TEM imaging) or 2% PFA (fluorescence imaging). Cells for TEM imaging were taken to the Electron Microscopy Core Imaging facility for further processing and imaging as described below. Cells for fluorescence *in situ* hybridization (FISH) imaging were processed as described below and imaged on a Zeiss Duo 5 confocal microscope and 5 consecutive Z stack slices were compressed to create images. Cells for histology and cell viability imaging were processed as described below and imaged on a Zeiss Duo 5 confocal microscope where 3 consecutive Z stack slices were compressed to create images (viability) or a Zeiss Primo Star (histology).

Hematoxylin and Eosin (H&E) staining. The transwell membrane was excised from the support by rinsing the cell surface with PBS and cutting the perimeter of the membrane with a No. 11 blade on a scalpel. The membrane was then placed between two 32x25x3mm biopsy pads and secured in a histology cassette. The cassette was immersed in 10% formalin fixative solution for 24h and then processed by the UMB Pathology Histology Core using SOP NH306. Briefly, slides were placed in hematoxylin, rinsed with water, dipped in acid alcohol, rinsed with water, then sequentially placed in 80% ethanol, eosin, 95% ethanol twice, 100% ethanol twice and xylene thrice. Mounting media and a coverslip were then added. Resultant slices were imaged at 100X on the Zeiss Primo Star microscope (Zeiss).

Fluorescence staining. Briefly, cells were rinsed once with 500µl of Dulbecco's Phosphate Buffered Saline (PBS), fixed with 4% paraformaldehyde (PFA) for 30 min and permeabilized with 200µl 0.25% Triton X-100 in PBS for 10 min, followed by treatment with 300µl 0.1% Triton X-100 in PBS/Fish skin gelatin (FSG) (0.66%) for 20 min. The cells were then stained for chlamydial IFUs with 10µl of 5µg/ml of mouse anti-human chlamydia LPS (primary Ab) (US Biological, MA) in Triton X-100/PBS/FSG solution for 90 min. Secondary antibody staining was done by adding 2µl of 200µg/ml of goat anti-mouse Alexa Fluor 488 in Triton X-100/PBS/FSG solution and incubated 60 min in the dark. Host cells were stained with 2µl of 500µg/ml Hoechst in Triton X-100/PBS/FSG solution for 10 min in the dark. Chlamydial inclusions stained green while host cells nuclei stained blue. Cells were imaged using a Zeiss Duo 5 confocal microscope and 3 consecutive Z stack slices were compressed to create images for analysis.

Transmission electron microscopy (TEM) staining. Cells were rinsed with PBS after removal of media and fixed in 500µl of 2% paraformaldehyde, 2.5% glutaraldehyde and 0.1 M PIPES

buffer (pH 7.4) for at least 1 hour. Cells were then washed with 500µl of 0.1 M PIPES, quenched with 500µl of 50mM glycine in 0.1 M PIPES buffer (pH 7) for 15 minutes, washed and post-fixed in 200µl of 1% (w/v) osmium tetroxide and 0.75% ferrocyanide in 0.1M PIPES buffer at 4°C for 60 min. Following washing, transwell membranes were sliced off the holding cup, stained with 200µl of 1% (w/v) uranyl acetate in water for 60 min, dehydrated by passage through a graduated ethanol series and embedded in spurr's resin (Electron Microscopy Sciences, PA) following the manufacturer's recommendations. Resin blocks were trimmed perpendicular to the monolayer grown on the transwell membrane. Ultrathin sections ~70nm thickness were cut on a Leica UC6 ultramicrotome (Leica Microsystems, Inc., Bannockburn, IL) and collected onto formva film coated SynapTek NOTCH-DOT grids (Electron Microscopy Sciences, Hatfield, PA) and examined in a Tecnai T12 transmission electron microscope (Thermo Fisher Scientific, formerly FEI. Co., Hillsboro, OR) operated at 80 keV. Digital images were acquired by using a bottom mount CCD camera and AMT600 software (Advanced Microscopy Techniques, Corp, Woburn, MA).

Fluorescence *in situ* hybridization (FISH) staining. Cells were stained using a protocol modified from Meaburn et al. [80]. Briefly, cells were rinsed and fixed overnight at 4°C with 2% PFA then incubated in 200µl of 0.5% saponin/ 0.5% Triton X100/ PBS mixture for 40 min. This was followed by the addition of 200µl of 1N HCL for 20 min, 2X SCC for 10 min and 50% formamide/2X SCC for 30 min incubations. Cells were then incubated in 300µl of the hybridization mix containing the FISH probe EUB338-ATT0 for 10 min at 85°C then overnight in a humidity box at 37°C. Cells were washed with 500µl of multiple buffers (a) 50% formamide/2X SSC buffer at 45°C, (b) 1X SSC buffer at 45°C and (c) 0.05% Tween-20 in 4X SSC buffer at room temperature. Cells were then incubated with 300µl of Hoechst at 1:500 for 10 min and mounted for imaging. Cells were imaged on the Zeiss Duo 5 microscope (Zeiss) using the 63X objective with 488 and 546 filters.

Viability staining. At 48h post-infection cells were incubated with 300µl of 4 µM Calcein-AM and 2 µM EthD-III from the Viability/Cytotoxicity Assay Kit for Animal Live and Dead cells (Biotium 30002-T) for 45 min at room temperature as per manufacturer's recommendations. Cells were imaged at 40X using the 488nm and 543nm excitation wavelengths on the Zeiss Duo 5 microscope (Zeiss). A composite overlay of 3 Z stack slices were used to create a 3D image.

ACKNOWLEDGEMENTS:

The authors would like to thank Dr. Alison Quayle for kindly providing the A2EN cell line, Dr. Ru-ching Hsia and the staff of the University of Maryland-Baltimore Electron Microscopy Core for preparing cells for EM imaging. Dr. Joseph Mauban of the University of Maryland-Baltimore Confocal Microscope Core for advice and assistance on the confocal microscope. University of Maryland School of Medicine's Center for Innovative Biomedical Resources, Histology Core and Cytokine Core – Baltimore, Maryland for providing advice, sectioning, and staining or running the samples for analysis.

FUNDING:

Research reported in this publication was supported by the National Institute for Allergy and Infectious Diseases of the National Institutes of Health under awards number U19AI084044 and U19AI158930.

AUTHOR CONTRIBUTIONS

J.R., P.M.B. and V.L.E designed research; V.L.E. and E.M. performed research; V.L.E. and E.M. analyzed data; V.L.E., J.R., P.M.B., J.P.G., and L.J.F. wrote the paper; J.R., J.P.G. and P.M.B. obtained funding.

CONFLICTS

J.R. is co-founder of LUCA Biologics, a biotechnology company focusing on translating microbiome research into live biotherapeutics drugs for women's health. All other authors declare that they have no competing interests.

REFERENCES

1. Hurley BP, McCormick BA. Translating tissue culture results into animal models: the case of Salmonella typhimurium. Trends Microbiol. 2003;11(12):562-9. Epub 2003/12/09. doi: 10.1016/j.tim.2003.10.002. PubMed PMID: 14659688.
2. Abbott A. Cell culture: biology's new dimension. Nature. 2003;424(6951):870-2. Epub 2003/08/22. doi: 10.1038/424870a. PubMed PMID: 12931155.
3. Barrila J, Radtke AL, Crabbé A, Sarker SF, Herbst-Kralovetz MM, Ott CM, et al. Organotypic 3D cell culture models: using the rotating wall vessel to study host–pathogen interactions. Nature Reviews Microbiology. 2010;8(11):791-801. doi: 10.1038/nrmicro2423.
4. Schmeichel KL, Bissell MJ. Modeling tissue-specific signaling and organ function in three dimensions. J Cell Sci. 2003;116(Pt 12):2377-88. Epub 2003/05/27. doi: 10.1242/jcs.00503. PubMed PMID: 12766184; PubMed Central PMCID: PMCPMC2933213.
5. Karolina Zuk A, Wen X, Dilworth S, Li D, Ghali L. Modeling and validating three dimensional human normal cervix and cervical cancer tissues in vitro. J Biomed Res. 2017;31(3):240-7. Epub 2017/08/16. doi: 10.7555/JBR.31.20160150. PubMed PMID: 28808216; PubMed Central PMCID: PMCPMC5460612.
6. Drummond CG, Nickerson CA, Coyne CB. A Three-Dimensional Cell Culture Model To Study Enterovirus Infection of Polarized Intestinal Epithelial Cells. mSphere. 2016;1(1). Epub 2016/06/16. doi: 10.1128/mSphere.00030-15. PubMed PMID: 27303677; PubMed Central PMCID: PMCPMC4863623.
7. Jonathan David NMS, Mitali Sarkar-Tyson. The use of a three-dimensional cell culture model to investigate host–pathogen interactions of *Francisella tularensis* in human lung epithelial cells. Microbes and Infection. 2014;16(9):735-45. Epub 4 May 2014.
8. Herbst-Kralovetz MM, Pyles RB, Ratner AJ, Sycuro LK, Mitchell C. New Systems for Studying Intercellular Interactions in Bacterial Vaginosis. J Infect Dis. 2016;214 Suppl 1:S6-S13. Epub 2016/07/28. doi: 10.1093/infdis/jiw130. PubMed PMID: 27449872; PubMed Central PMCID: PMCPMC4957508.
9. Raterman EL, Jerse AE. Female Mouse Model of Neisseria gonorrhoeae Infection. Methods Mol Biol. 2019;1997:413-29. Epub 2019/05/24. doi: 10.1007/978-1-4939-9496-0_24. PubMed PMID: 31119637.
10. Llewellyn GN, Seclen E, Wietgrefe S, Liu S, Chateau M, Pei H, et al. Humanized Mouse Model of HIV-1 Latency with Enrichment of Latent Virus in PD-1(+) and TIGIT(+) CD4 T Cells. J Virol. 2019;93(10). Epub 2019/03/08. doi: 10.1128/JVI.02086-18. PubMed PMID: 30842333; PubMed Central PMCID: PMCPMC6498059.
11. Lavender KJ, Pace C, Sutter K, Messer RJ, Pouncey DL, Cummins NW, et al. An advanced BLT-humanized mouse model for extended HIV-1 cure studies. AIDS. 2018;32(1):1-10. Epub 2017/11/08. doi: 10.1097/QAD.0000000000001674. PubMed PMID: 29112072; PubMed Central PMCID: PMCPMC5718929.
12. Dutow P, Wask L, Bothe M, Fehlhaber B, Laudeley R, Rheinheimer C, et al. An optimized, fast-to-perform mouse lung infection model with the human pathogen Chlamydia trachomatis for in vivo screening of antibiotics, vaccine candidates and modified host-pathogen interactions. Pathogens and disease. 2016;74(2). Epub 2015/12/18. doi: 10.1093/femspd/ftv120. PubMed PMID: 26676260.
13. Pal S, Tifrea DF, Zhong G, de la Maza LM. Transcervical Inoculation with Chlamydia trachomatis Induces Infertility in HLA-DR4 Transgenic and Wild-Type Mice. Infect Immun. 2018;86(1). Epub 2017/10/19. doi: 10.1128/IAI.00722-17. PubMed PMID: 29038126; PubMed Central PMCID: PMCPMC5736824.

14. Lutz-Wohlgroth L, Becker A, Brugnera E, Huat ZL, Zimmermann D, Grimm F, et al. Chlamydiales in guinea-pigs and their zoonotic potential. J Vet Med A Physiol Pathol Clin Med. 2006;53(4):185-93. Epub 2006/04/25. doi: 10.1111/j.1439-0442.2006.00819.x. PubMed PMID: 16629952.
15. Rank RG, Sanders MM. Pathogenesis of endometritis and salpingitis in a guinea pig model of chlamydial genital infection. Am J Pathol. 1992;140(4):927-36. Epub 1992/04/01. PubMed PMID: 1562052; PubMed Central PMCID: PMCPMC1886353.
16. Shaw JH, Behar AR, Snider TA, Allen NA, Lutter EI. Comparison of Murine Cervicovaginal Infection by Chlamydial Strains: Identification of Extrusions Shed In vivo. Front Cell Infect Microbiol. 2017;7:18. Epub 2017/02/22. doi: 10.3389/fcimb.2017.00018. PubMed PMID: 28217555; PubMed Central PMCID: PMCPMC5289954.
17. Zhang YX, Fox JG, Ho Y, Zhang L, Stills HF, Jr., Smith TF. Comparison of the major outer-membrane protein (MOMP) gene of mouse pneumonitis (MoPn) and hamster SFPD strains of Chlamydia trachomatis with other Chlamydia strains. Mol Biol Evol. 1993;10(6):1327-42. Epub 1993/11/01. doi: 10.1093/oxfordjournals.molbev.a040079. PubMed PMID: 8277858.
18. Harrington H, Cato P, Salazar F, Wilkinson M, Knox A, Haycock JW, et al. Immunocompetent 3D model of human upper airway for disease modeling and in vitro drug evaluation. Mol Pharm. 2014;11(7):2082-91. Epub 2014/03/19. doi: 10.1021/mp5000295. PubMed PMID: 24628276; PubMed Central PMCID: PMCPMC4086737.
19. Barrila J, Crabbe A, Yang J, Franco K, Nydam SD, Forsyth RJ, et al. Modeling Host-Pathogen Interactions in the Context of the Microenvironment: Three-Dimensional Cell Culture Comes of Age. Infect Immun. 2018;86(11). Epub 2018/09/06. doi: 10.1128/IAI.00282-18. PubMed PMID: 30181350; PubMed Central PMCID: PMCPMC6204695.
20. Gargus ES, Rogers HB, McKinnon KE, Edmonds ME, Woodruff TK. Engineered reproductive tissues. Nat Biomed Eng. 2020;4(4):381-93. Epub 2020/04/07. doi: 10.1038/s41551-020-0525-x. PubMed PMID: 32251392; PubMed Central PMCID: PMCPMC7416444.
21. Orabi H, Saba I, Rousseau A, Bolduc S. Novel three-dimensional autologous tissue-engineered vaginal tissues using the self-assembly technique. Translational research : the journal of laboratory and clinical medicine. 2017;180:22-36. Epub 2016/08/21. doi: 10.1016/j.trsl.2016.07.019. PubMed PMID: 27543901.
22. Zhu Y, Yang Y, Guo J, Dai Y, Ye L, Qiu J, et al. Ex vivo 2D and 3D HSV-2 infection model using human normal vaginal epithelial cells. Oncotarget. 2017;8(9):15267-82. Epub 2017/02/02. doi: 10.18632/oncotarget.14840. PubMed PMID: 28146426; PubMed Central PMCID: PMCPMC5362485.
23. Xiao S, Coppeta JR, Rogers HB, Isenberg BC, Zhu J, Olalekan SA, et al. A microfluidic culture model of the human reproductive tract and 28-day menstrual cycle. Nature communications. 2017;8:14584. Epub 2017/03/30. doi: 10.1038/ncomms14584. PubMed PMID: 28350383; PubMed Central PMCID: PMCPMC5379057.
24. Hjelm BE, Berta AN, Nickerson CA, Arntzen CJ, Herbst-Kralovetz MM. Development and characterization of a three-dimensional organotypic human vaginal epithelial cell model. Biol Reprod. 2010;82(3):617-27. Epub 2009/12/17. doi: 10.1095/biolreprod.109.080408. PubMed PMID: 20007410; PubMed Central PMCID: PMCPMC6366157.
25. Ogawa-Tominaga M, Umezu T, Nakajima T, Tomooka Y. Stratification of mouse vaginal epithelium. 1. Development of three-dimensional models in vitro with clonal cell lines. Biol Reprod. 2018;99(4):718-26. Epub 2018/05/17. doi: 10.1093/biolre/ioy114. PubMed PMID: 29767686.

564 26. Millar-Haskell CS, Dang AM, Gleghorn JP. Coupling synthetic biology and programmable
565 materials to construct complex tissue ecosystems. MRS Commun. 2019;9(2):421-32. Epub
566 2019/09/06. doi: 10.1557/mrc.2019.69. PubMed PMID: 31485382; PubMed Central PMCID:
567 PMCPMC6724541.
568 27. Pyles RB, Vincent KL, Baum MM, Elsom B, Miller AL, Maxwell C, et al. Cultivated vaginal
569 microbiomes alter HIV-1 infection and antiretroviral efficacy in colonized epithelial multilayer
570 cultures. PLoS One. 2014;9(3):e93419. Epub 2014/03/29. doi: 10.1371/journal.pone.0093419.
571 PubMed PMID: 24676219; PubMed Central PMCID: PMCPMC3968159.
572 28. Hjelm BE, Berta AN, Nickerson CA, Arntzen CJ, Herbst-Kralovetz MM. Development and
573 Characterization of a Three-Dimensional Organotypic Human Vaginal Epithelial Cell Model.
574 Biology of Reproduction. 2010;82(3):617-27. doi: 10.1095/biolreprod.109.080408.
575 29. Medina-Colorado AA, Vincent KL, Miller AL, Maxwell CA, Dawson LN, Olive T, et al. Vaginal
576 ecosystem modeling of growth patterns of anaerobic bacteria in microaerophilic conditions.
577 Anaerobe. 2017;45:10-8. Epub 2017/05/01. doi: 10.1016/j.anaerobe.2017.04.014. PubMed
578 PMID: 28456518; PubMed Central PMCID: PMCPMC5726262.
579 30. Amerson-Brown MH, Miller AL, Maxwell CA, White MM, Vincent KL, Bourne N, et al.
580 Cultivated Human Vaginal Microbiome Communities Impact Zika and Herpes Simplex Virus
581 Replication in ex vivo Vaginal Mucosal Cultures. Front Microbiol. 2018;9:3340. Epub
582 2019/01/30. doi: 10.3389/fmicb.2018.03340. PubMed PMID: 30692980; PubMed Central
583 PMCID: PMCPMC6340164.
584 31. Nogueira AT, Braun KM, Carabeo RA. Characterization of the Growth of Chlamydia
585 trachomatis in In Vitro-Generated Stratified Epithelium. Front Cell Infect Microbiol. 2017;7:438.
586 Epub 2017/10/27. doi: 10.3389/fcimb.2017.00438. PubMed PMID: 29067282; PubMed Central
587 PMCID: PMCPMC5641298.
588 32. Gorwood J, Bourgeois C, Mantecon M, Atlan M, Pourcher V, Pourcher G, et al. Impact of
589 HIV/simian immunodeficiency virus infection and viral proteins on adipose tissue fibrosis and
590 adipogenesis. AIDS. 2019;33(6):953-64. Epub 2019/04/05. doi:
591 10.1097/QAD.0000000000002168. PubMed PMID: 30946149.
592 33. Imle A, Kumberger P, Schnellbacher ND, Fehr J, Carrillo-Bustamante P, Ales J, et al.
593 Experimental and computational analyses reveal that environmental restrictions shape HIV-1
594 spread in 3D cultures. Nat Commun. 2019;10(1):2144. Epub 2019/05/16. doi: 10.1038/s41467-
595 019-09879-3. PubMed PMID: 31086185; PubMed Central PMCID: PMCPMC6514199.
596 34. Heydarian M, Yang T, Schweinlin M, Steinke M, Walles H, Rudel T, et al. Biomimetic
597 Human Tissue Model for Long-Term Study of Neisseria gonorrhoeae Infection. Frontiers in
598 Microbiology. 2019;10:1740. doi: 10.3389/fmicb.2019.01740. PubMed PMID: 31417529;
599 PubMed Central PMCID: PMCPMC6685398.
600 35. Radtke AL, Herbst-Kralovetz MM. Culturing and Applications of Rotating Wall Vessel
601 Bioreactor Derived 3D Epithelial Cell Models. Journal of visualized experiments : JoVE.
602 2012;(62). doi: 10.3791/3868.
603 36. Laniewski P, Gomez A, Hire G, So M, Herbst-Kralovetz MM. Human Three-Dimensional
604 Endometrial Epithelial Cell Model To Study Host Interactions with Vaginal Bacteria and Neisseria
605 gonorrhoeae. Infect Immun. 2017;85(3). Epub 2017/01/06. doi: 10.1128/IAI.01049-16. PubMed
606 PMID: 28052997; PubMed Central PMCID: PMCPMC5328489.
607 37. Laniewski P, Herbst-Kralovetz MM. Analysis of Host Responses to Neisseria gonorrhoeae
608 Using a Human Three-Dimensional Endometrial Epithelial Cell Model. Methods Mol Biol.
609 2019;1997:347-61. Epub 2019/05/24. doi: 10.1007/978-1-4939-9496-0_20. PubMed PMID:
610 31119633.

611 38. Heydarian M, Yang T, Schweinlin M, Steinke M, Walles H, Rudel T, et al. Biomimetic
612 Human Tissue Model for Long-Term Study of Neisseria gonorrhoeae Infection. Front Microbiol.
613 2019;10:1740. Epub 2019/08/17. doi: 10.3389/fmicb.2019.01740. PubMed PMID: 31417529;
614 PubMed Central PMCID: PMCPMC6685398.
615 39. Ilhan ZE, Laniewski P, Thomas N, Roe DJ, Chase DM, Herbst-Kralovetz MM. Deciphering
616 the complex interplay between microbiota, HPV, inflammation and cancer through
617 cervicovaginal metabolic profiling. EBioMedicine. 2019;44:675-90. Epub 2019/04/28. doi:
618 10.1016/j.ebiom.2019.04.028. PubMed PMID: 31027917; PubMed Central PMCID:
619 PMCPMC6604110.
620 40. Doerflinger SY, Throop AL, Herbst-Kralovetz MM. Bacteria in the Vaginal Microbiome
621 Alter the Innate Immune Response and Barrier Properties of the Human Vaginal Epithelia in a
622 Species-Specific Manner. The Journal of Infectious Diseases. 2014. doi: 10.1093/infdis/jiu004.
623 41. Picollet-D'hahan N, Zuchowska A, Lemeunier I, Le Gac S. Multiorgan-on-a-Chip: A
624 Systemic Approach To Model and Decipher Inter-Organ Communication. Trends Biotechnol.
625 2021;39(8):788-810. Epub 2021/02/06. doi: 10.1016/j.tibtech.2020.11.014. PubMed PMID:
626 33541718.
627 42. Tantengco OAG, Richardson LS, Medina PMB, Han A, Menon R. Organ-on-chip of the
628 cervical epithelial layer: A platform to study normal and pathological cellular remodeling of the
629 cervix. FASEB J. 2021;35(4):e21463. Epub 2021/03/11. doi: 10.1096/fj.202002590RRR. PubMed
630 PMID: 33689188; PubMed Central PMCID: PMCPMC8193817.
631 43. Choi NW, Cabodi M, Held B, Gleghorn JP, Bonassar LJ, Stroock AD. Microfluidic scaffolds
632 for tissue engineering. Nat Mater. 2007;6(11):908-15. Epub 2007/10/02. doi:
633 10.1038/nmat2022. PubMed PMID: 17906630.
634 44. Cabodi M, Choi NW, Gleghorn JP, Lee CS, Bonassar LJ, Stroock AD. A microfluidic
635 biomaterial. J Am Chem Soc. 2005;127(40):13788-9. Epub 2005/10/06. doi: 10.1021/ja054820t.
636 PubMed PMID: 16201789.
637 45. Edwards VL, Smith SB, McComb EJ, Tamarelle J, Ma B, Humphrys MS, et al. The
638 Cervicovaginal Microbiota-Host Interaction Modulates Chlamydia trachomatis Infection. mBio.
639 2019;10(4). Epub 2019/08/15. doi: 10.1128/mBio.01548-19. PubMed PMID: 31409678;
640 PubMed Central PMCID: PMCPMC6692509.
641 46. Buckner LR, Schust DJ, Ding J, Nagamatsu T, Beatty W, Chang TL, et al. Innate immune
642 mediator profiles and their regulation in a novel polarized immortalized epithelial cell model
643 derived from human endocervix. Journal of reproductive immunology. 2011;92(1-2):8-20. doi:
644 10.1016/j.jri.2011.08.002. PubMed PMID: 21943934.
645 47. Nunn KL, Wang YY, Harit D, Humphrys MS, Ma B, Cone R, et al. Enhanced Trapping of HIV-
646 1 by Human Cervicovaginal Mucus Is Associated with Lactobacillus crispatus-Dominant
647 Microbiota. mBio. 2015;6(5):e01084-15. doi: 10.1128/mBio.01084-15. PubMed PMID:
648 26443453; PubMed Central PMCID: PMC4611035.
649 48. Eggert-Kruse W, Botz I, Pohl S, Rohr G, Strowitzki T. Antimicrobial activity of human
650 cervical mucus. Hum Reprod. 2000;15(4):778-84. Epub 2000/03/31. doi:
651 10.1093/humrep/15.4.778. PubMed PMID: 10739819.
652 49. Powell DW. Barrier function of epithelia. Am J Physiol. 1981;241(4):G275-88. Epub
653 1981/10/01. doi: 10.1152/ajpgi.1981.241.4.G275. PubMed PMID: 7032321.
654 50. Adnane M, Meade KG, O'Farrelly C. Cervico-vaginal mucus (CVM) - an accessible source of
655 immunologically informative biomolecules. Vet Res Commun. 2018;42(4):255-63. Epub
656 2018/08/18. doi: 10.1007/s11259-018-9734-0. PubMed PMID: 30117040; PubMed Central
657 PMCID: PMCPMC6244541.

658 51. Han L, Andrews W, Wong K, Jensen JT. Conditionally Reprogrammed Macaque
659 Endocervical Cells Retain Steroid Receptor Expression and Produce Mucus. Biol Reprod. 2020.
660 Epub 2020/04/02. doi: 10.1093/biolre/ioaa039. PubMed PMID: 32232331.
661 52. Anderson DJ, Marathe J, Pudney J. The structure of the human vaginal stratum corneum
662 and its role in immune defense. American journal of reproductive immunology. 2014;71(6):618-
663 23. Epub 2014/03/26. doi: 10.1111/aji.12230. PubMed PMID: 24661416; PubMed Central
664 PMCID: PMCPMC4024347.
665 53. Buckner LR, Lewis ME, Greene SJ, Foster TP, Quayle AJ. Chlamydia trachomatis infection
666 results in a modest pro-inflammatory cytokine response and a decrease in T cell chemokine
667 secretion in human polarized endocervical epithelial cells. CYTOKINE. 2013;63(2):151-65. doi:
668 10.1016/j.cyto.2013.04.022. PubMed PMID: 23673287; PubMed Central PMCID:
669 PMCPMC3703936.
670 54. Yang C, Briones M, Chiou J, Lei L, Patton MJ, Ma L, et al. Chlamydia trachomatis
671 Lipopolysaccharide Evades the Canonical and Noncanonical Inflammatory Pathways To Subvert
672 Innate Immunity. mBio. 2019;10(2). Epub 2019/04/25. doi: 10.1128/mBio.00595-19. PubMed
673 PMID: 31015326; PubMed Central PMCID: PMCPMC6479002.
674 55. Hwang LY, Scott ME, Ma Y, Moscicki AB. Diversity of Cervicovaginal Cytokine Response to
675 Incident Chlamydia trachomatis Infection Among a Prospective Cohort of Young Women. Am J
676 Reprod Immunol. 2015;74(3):228-36. Epub 2015/05/21. doi: 10.1111/aji.12401. PubMed PMID:
677 25989718; PubMed Central PMCID: PMCPMC4564257.
678 56. Bua A, Cannas S, Zanetti S, Molicotti P. Levels of different cytokines in women and men
679 with asymptomatic genital infection caused by Chlamydia. J Infect Dev Ctries. 2019;13(9):847-
680 50. Epub 2020/02/20. doi: 10.3855/jidc.9810. PubMed PMID: 32074096.
681 57. Unemo M, Seifert HS, Hook EW, 3rd, Hawkes S, Ndowa F, Dillon JR. Gonorrhoea. Nat Rev
682 Dis Primers. 2019;5(1):79. Epub 2019/11/23. doi: 10.1038/s41572-019-0128-6. PubMed PMID:
683 31754194.
684 58. Batteiger BE, Fraiz J, Newhall WJ, Katz BP, Jones RB. Association of recurrent chlamydial
685 infection with gonorrhea. J Infect Dis. 1989;159(4):661-9. Epub 1989/04/01. doi:
686 10.1093/infdis/159.4.661. PubMed PMID: 2926160.
687 59. Creighton S, Tenant-Flowers M, Taylor CB, Miller R, Low N. Co-infection with gonorrhoea
688 and chlamydia: how much is there and what does it mean? Int J STD AIDS. 2003;14(2):109-13.
689 Epub 2003/03/29. doi: 10.1258/095646203321156872. PubMed PMID: 12662389.
690 60. Edwards VL, Wang L-C, Dawson V, Stein DC, Song W. Neisseria gonorrhoeae breaches the
691 apical junction of polarized epithelial cells for transmigration by activating EGFR. Cellular
692 Microbiology. 2013;15(6):1042-57. doi: 10.1111/cmi.12099. PubMed PMID:
693 WOS:000318931800014.
694 61. Jarvis GA, Li J, Swanson KV. Invasion of human mucosal epithelial cells by Neisseria
695 gonorrhoeae upregulates expression of intercellular adhesion molecule 1 (ICAM-1). Infect
696 Immun. 1999;67(3):1149-56. Epub 1999/02/20. PubMed PMID: 10024555; PubMed Central
697 PMCID: PMCPMC96441.
698 62. Spurbeck RR, Arvidson CG. Inhibition of Neisseria gonorrhoeae epithelial cell interactions
699 by vaginal Lactobacillus species. Infection and immunity. 2008;76(7):3124-30. doi:
700 10.1128/IAI.00101-08. PubMed PMID: 18411284; PubMed Central PMCID: PMCPMC2446695.
701 63. Griffiss JM, Lammel CJ, Wang J, Dekker NP, Brooks GF. Neisseria gonorrhoeae coordinately
702 uses Pili and Opa to activate HEC-1-B cell microvilli, which causes engulfment of the gonococci.
703 Infect Immun. 1999;67(7):3469-80. Epub 1999/06/22. PubMed PMID: 10377128; PubMed
704 Central PMCID: PMCPMC116533.

64. Ma B, Forney LJ, Ravel J. Vaginal microbiome: rethinking health and disease. Annu Rev Microbiol. 2012;66:371-89. Epub 2012/07/04. doi: 10.1146/annurev-micro-092611-150157. PubMed PMID: 22746335.
65. McKinnon LR, Achilles S, Bradshaw CS, Burgener A, Crucitti T, Fredricks DN, et al. The evolving facets of bacterial vaginosis: implications for HIV transmission. AIDS Res Hum Retroviruses. 2019. Epub 2019/01/15. doi: 10.1089/AID.2018.0304. PubMed PMID: 30638028.
66. Witkin SS, Mendes-Soares H, Linhares IM, Jayaram A, Ledger WJ, Forney LJ. Influence of vaginal bacteria and D- and L-lactic acid isomers on vaginal extracellular matrix metalloproteinase inducer: implications for protection against upper genital tract infections. MBio. 2013;4(4). Epub 2013/08/06. doi: 10.1128/mBio.00460-13. PubMed PMID: 23919998; PubMed Central PMCID: PMCPMC3735189.
67. Boskey ER, Cone RA, Whaley KJ, Moench TR. Origins of vaginal acidity: high D/L lactate ratio is consistent with bacteria being the primary source. Hum Reprod. 2001;16(9):1809-13. PubMed PMID: 11527880.
68. O'Hanlon DE, Moench TR, Cone RA. Vaginal pH and microbicidal lactic acid when lactobacilli dominate the microbiota. PLoS One. 2013;8(11):e80074. Epub 2013/11/06. doi: 10.1371/journal.pone.0080074. PubMed PMID: 24223212; PubMed Central PMCID: PMCPMC3819307.
69. Barrila J, Radtke AL, Crabbe A, Sarker SF, Herbst-Kralovetz MM, Ott CM, et al. Organotypic 3D cell culture models: using the rotating wall vessel to study host-pathogen interactions. Nat Rev Microbiol. 2010;8(11):791-801. Epub 2010/10/16. doi: 10.1038/nrmicro2423. PubMed PMID: 20948552.
70. David J, Sayer NM, Sarkar-Tyson M. The use of a three-dimensional cell culture model to investigate host-pathogen interactions of Francisella tularensis in human lung epithelial cells. Microbes Infect. 2014;16(9):735-45. Epub 2014/05/07. doi: 10.1016/j.micinf.2014.04.001. PubMed PMID: 24796635.
71. Aiyar A, Quayle AJ, Buckner LR, Sherchand SP, Chang TL, Zea AH, et al. Influence of the tryptophan-indole-IFNgamma axis on human genital Chlamydia trachomatis infection: role of vaginal co-infections. Front Cell Infect Microbiol. 2014;4:72. Epub 2014/06/12. doi: 10.3389/fcimb.2014.00072. PubMed PMID: 24918090; PubMed Central PMCID: PMCPMC4042155.
72. Ziklo N, Huston WM, Taing K, Katouli M, Timms P. In vitro rescue of genital strains of Chlamydia trachomatis from interferon-gamma and tryptophan depletion with indole-positive, but not indole-negative Prevotella spp. BMC Microbiol. 2016;16(1):286. Epub 2016/12/05. doi: 10.1186/s12866-016-0903-4. PubMed PMID: 27914477; PubMed Central PMCID: PMCPMC5135834.
73. Ziklo N, Vidgen ME, Taing K, Huston WM, Timms P. Dysbiosis of the Vaginal Microbiota and Higher Vaginal Kynurenine/Tryptophan Ratio Reveals an Association with Chlamydia trachomatis Genital Infections. Front Cell Infect Microbiol. 2018;8:1. Epub 2018/02/07. doi: 10.3389/fcimb.2018.00001. PubMed PMID: 29404279; PubMed Central PMCID: PMCPMC5778109.
74. Shemer Y, Sarov I. Inhibition of growth of Chlamydia trachomatis by human gamma interferon. Infect Immun. 1985;48(2):592-6. Epub 1985/05/01. PubMed PMID: 2985506; PubMed Central PMCID: PMC261392.
75. Yildirim S, Yeoman CJ, Janga SC, Thomas SM, Ho M, Leigh SR, et al. Primate vaginal microbiomes exhibit species specificity without universal Lactobacillus dominance. The ISME Journal. 2014;8(12):2431-44. doi: 10.1038/ismej.2014.90.

752 76. Stumpf RM, Wilson BA, Rivera A, Yildirim S, Yeoman CJ, Polk JD, et al. The primate vaginal
753 microbiome: Comparative context and implications for human health and disease. American
754 Journal of Physical Anthropology. 2013. doi: 10.1002/ajpa.22395. PubMed PMID: 24166771.
755 77. Miller EA, Beasley DE, Dunn RR, Archie EA. Lactobacilli Dominance and Vaginal pH: Why
756 Is the Human Vaginal Microbiome Unique? Front Microbiol. 2016;7:1936. Epub 2016/12/23. doi:
757 10.3389/fmicb.2016.01936. PubMed PMID: 28008325; PubMed Central PMCID:
758 PMCPMC5143676.
759 78. Tan C, Hsia RC, Shou H, Carrasco JA, Rank RG, Bavoil PM. Variable expression of surface-
760 exposed polymorphic membrane proteins in in vitro-grown Chlamydia trachomatis. Cell
761 Microbiol. 2010;12(2):174-87. doi: 10.1111/j.1462-5822.2009.01389.x. PubMed PMID:
762 19811502; PubMed Central PMCID: PMCPMC3073146.
763 79. Reeve P, Owen J, Oriel JD. Laboratory procedures for the isolation of chlamydia
764 trachomatis from the human genital tract. J Clin Pathol. 1975;28(11):910-4. Epub 1975/11/01.
765 doi: 10.1136/jcp.28.11.910. PubMed PMID: 1236632; PubMed Central PMCID: PMCPMC475892.
766 80. Meaburn KJ. Fluorescence in situ hybridization on 3D cultures of tumor cells. Methods
767 Mol Biol. 2010;659:323-36. Epub 2010/09/03. doi: 10.1007/978-1-60761-789-1_25. PubMed
768 PMID: 20809324.
769 81. Ball LM, Criss AK. Constitutively Opa-expressing and Opa-deficient neisseria gonorrhoeae
770 strains differentially stimulate and survive exposure to human neutrophils. Journal of
771 bacteriology. 2013;195(13):2982-90. doi: 10.1128/JB.00171-13. PubMed PMID: 23625842;
772 PubMed Central PMCID: PMCPMC3697530.
773 82. Smirnov A, Daily KP, Criss AK. Assembly of NADPH oxidase in human neutrophils is
774 modulated by the opacity-associated protein expression State of Neisseria gonorrhoeae. Infect
775 Immun. 2014;82(3):1036-44. Epub 2013/12/18. doi: 10.1128/IAI.00881-13. PubMed PMID:
776 24343654; PubMed Central PMCID: PMCPMC3957997.
777 83. White LA, Kellogg DS, Jr. Neisseria Gonorrhoeae Identification in Direct Smears by a
778 Fluorescent Antibody-Counterstain Method. Appl Microbiol. 1965;13:171-4. Epub 1965/03/01.
779 PubMed PMID: 14325874; PubMed Central PMCID: PMCPMC1058216.
780
781
782

Supplemental Materials

Transwell inserts (Corning #3472)

12 well plates (Corning #3513)

9" Glass pipettes (Corning #7095D)

Countess Automated Cell Counter (Invitrogen #C10227)

Mouse anti-human chlamydia LPS (US Biological #C4250-51F)

Goat anti-mouse Alexa Fluor 488 (Invitrogen #A-11029)

Rabbit anti-human MUC5B (Invitrogen #PA5-82342)

Goat anti-rabbit Alexa Fluor 488 (Invitrogen #A-11034)

Hoechst (Invitrogen #H3570)

FISH probe - EUB338-ATTO [5'-/565/GCT GCC TCC CGT AGG AGT-3'] (Invitrogen)

Histology fixative – 10% formalin solution (Sigma #HT501128)

D/L Lactic acid assay kit (R-Biopharm #11 112 821 035)

Rat tail collagen – 100mg (Corning #354236)

10X RPMI media (Sigma #R1145)

Sterile tissue culture water (Cellgro #25-055-CM)

1M NaOH – sterile filtered (Sigma #S5881)

0.25% Trypsin (Gibco #25200-056)

BJ human fibroblasts (ATCC #CRL 2522)

BJ complete media - DMEM media (Cellgro #15-013-CV) supplemented with 10% FBS (Sigma #F4135)

A2EN cervical epithelial cells (kindly provided by Dr. Allsion Quayle [46])

A2EN complete media - EpiLife media (Gibco #MEPICFPRF) with 100X EDGS supplement (Gibco #S-012-5) and 100X L glutamine (Lonza #17-605E)

VK2/E6/E7 human vaginal epithelial cells (ATCC #CRL 2616)

VK2 complete media - Keratinoctye-SFM (with BPE and EGF) (Gibco 310725-018) supplemented with Calcium chloride (Amresco #E506) and 100X L glutamine (Lonza #17-605E)

HeLa cervical epithelial cells (ATCC #CCL2)

HeLa complete media - Dulbecco's modified Eagle's medium (Corning #15-013-CV) supplemented with 10% FBS (Sigma #F4135)

HEC-1-B endometrial cells (ATCC #HTB-113)

HEC-1-B complete media – MEM alpha (1X) + GlutMaAX (GIBCO #32561-037) supplemented with 10% FBS (Sigma #F4135)

Chlamydia trachomatis serovar LGV II strain 434 (ATCC #VR 902B)

Neisseria gonorrhoeae strain FA1090 – wildtype and isogenic mutants (kindly provided by Dr. Alison Criss [81, 82]

Lactobacillus crispatus (ATCC #33197)

Lactobacillus iners (ATCC #55195)

Gardnerella vaginalis (ATCC #14018)

Difco GC medium base (BD #228920) with 1% Kelloggs supplement prepared as per White and Kellogg [83].

Bacteriological agar (Amresco #J637)

NYCIII medium: 10 g/L proteose peptone, 10 g/l beef extract, 5 g/l yeast extract, 5 g/L NaCl, 1.2 g/L $MgSO_4$, 2 g/L $MnSO_4.H_2O$, 5.7 g/L K_2HPO_4, 20 g/L glucose, 10% FBS.

Tryptic Soy Broth (Fluka #T8907) supplemented with 5% Horse serum (GIBCO #26050-088)

Figures and Figure Legends:

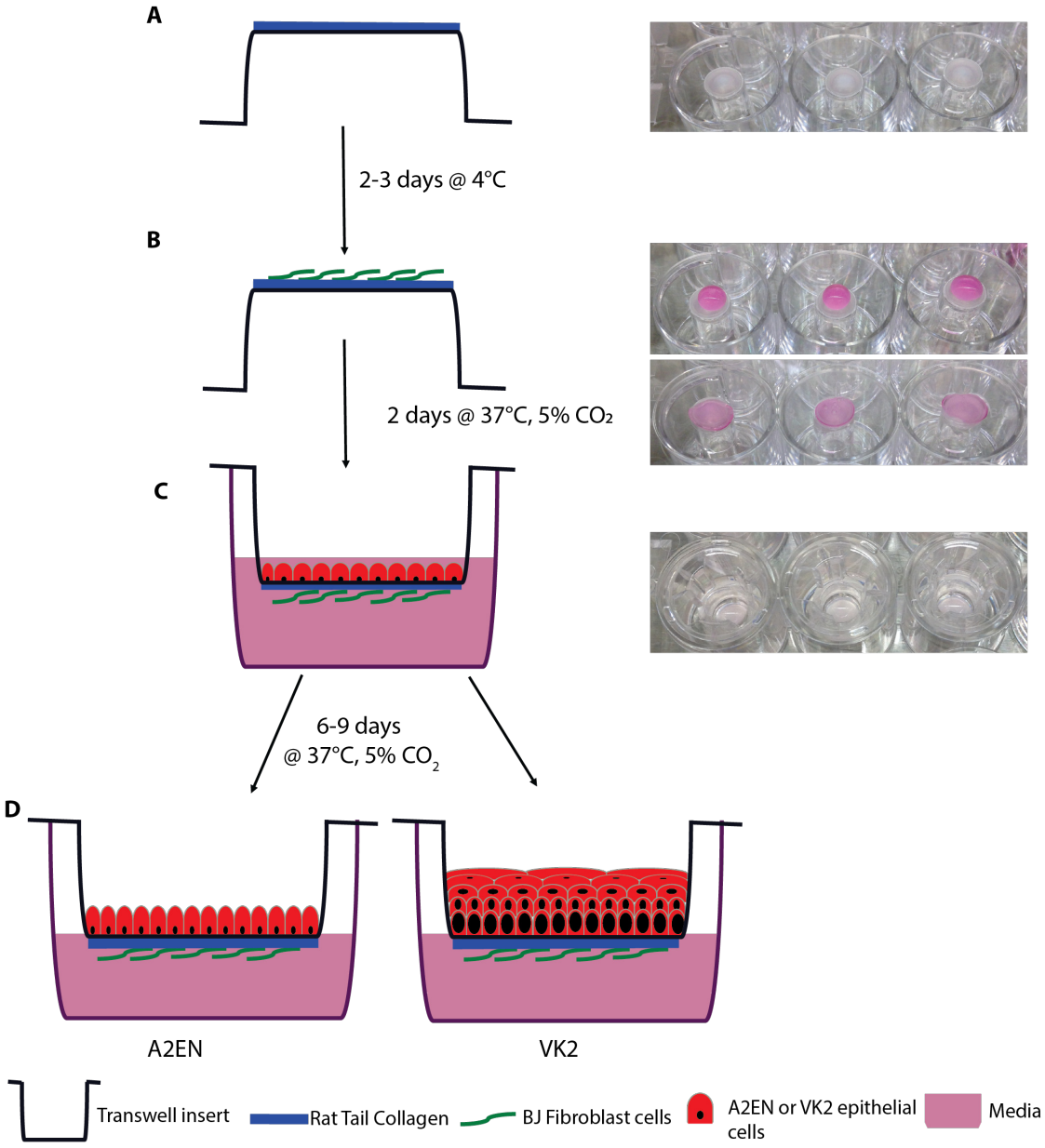

FIG 1 Model setup. 70µl of collagen was added to the basal portion of the inverted transwell (A) and stored at 4°C. BJ's were added to the basal membrane 2-3 days later at $3x10^4$ in a volume of 80-100µl and incubated at 37°C, 5%CO_2 (B). Epithelial cells (A2EN or VK2) were apically added at $1X10^5$ in a volume of 50-200µl (C). After 6-9 days incubation at 37°C, 5%CO_2 cells were ready to be used in experiments.

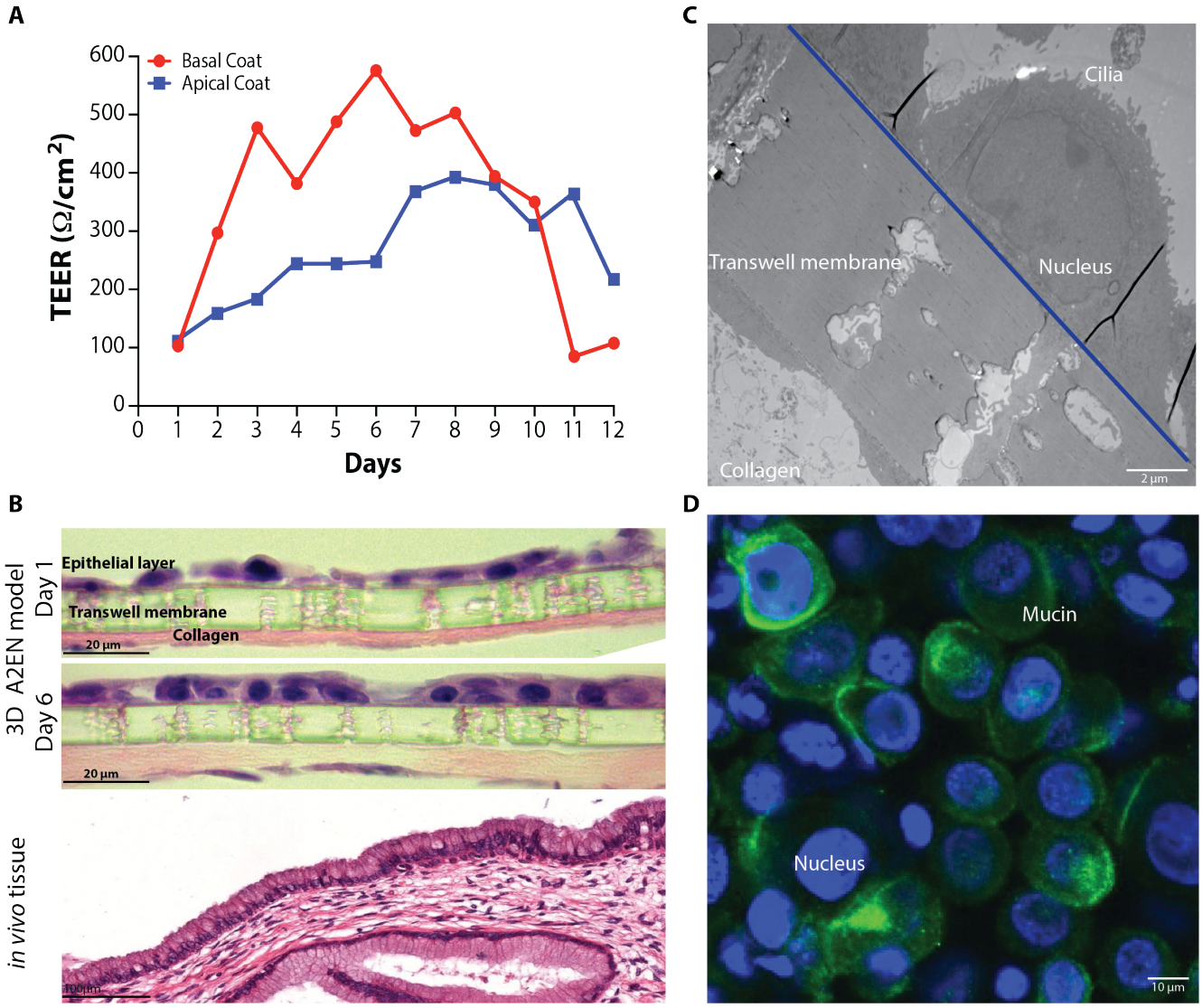

FIG 2 Characterization of the 3D cervical epithelium model (A2EN). Transepithelial resistance values over the course of A2EN epithelial cell transwell 3D model set up (A). Histology (H&E) imaging (B) and electron microscopy (TEM) imaging (C) of the epithelial cells of the model 6 days post set up. Confocal imaging of mucin gel formation (MUC-5B) on the model 6 days post set up (D).

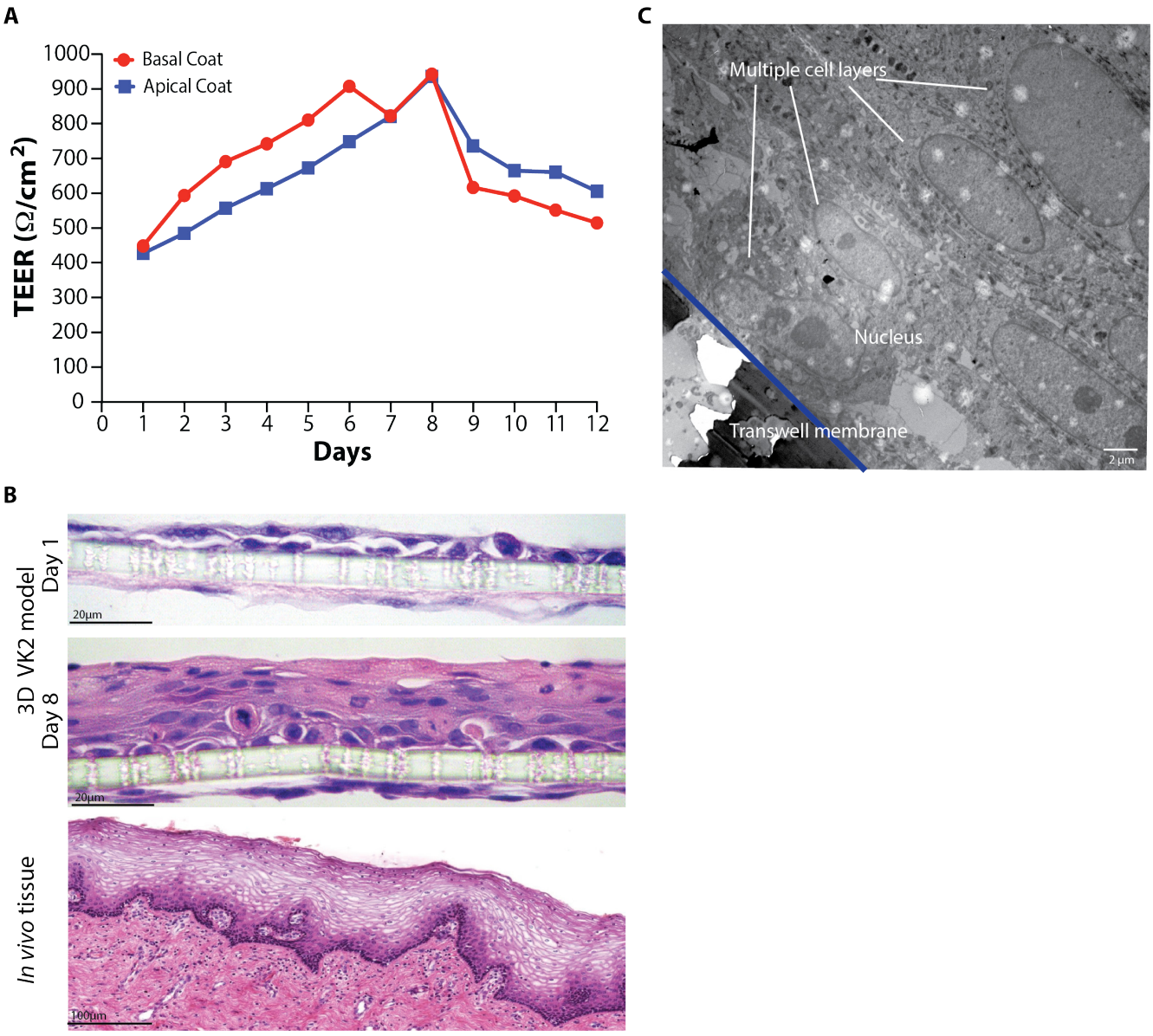

FIG 3 Characterization of the 3D vaginal epithelium model (VK2). Transepithelial resistance values over the course of VK2 epithelial cell transwell 3D model set up (A). Histology (H&E) imaging (B) and electron microscopy (TEM) imaging (C) of the epithelial cells of the model 8 days post set up.

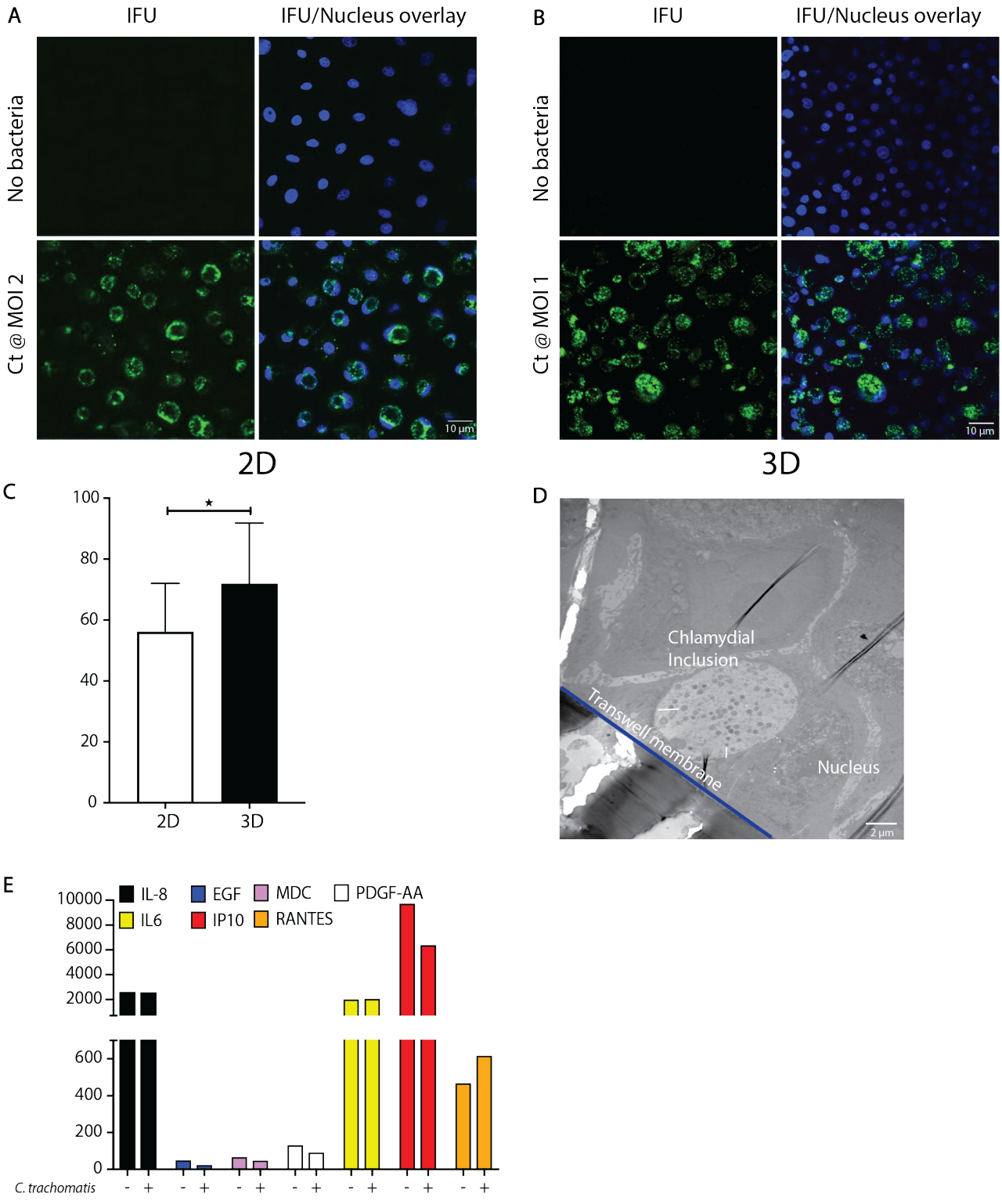

FIG 4 Infection of the 3D cervical model (A2EN) by *C. trachomatis*. Analysis of chlamydial infectivity on the conventional 2D (coverslip) model by fluorescent imaging (A) compared to the 3D (transwell) model (B) and resultant enumeration of infected cells (C). TEM image of infected cells on the 3D model (D). Cytokine profile of uninfected as compared to infected 3D cervical cells (E).

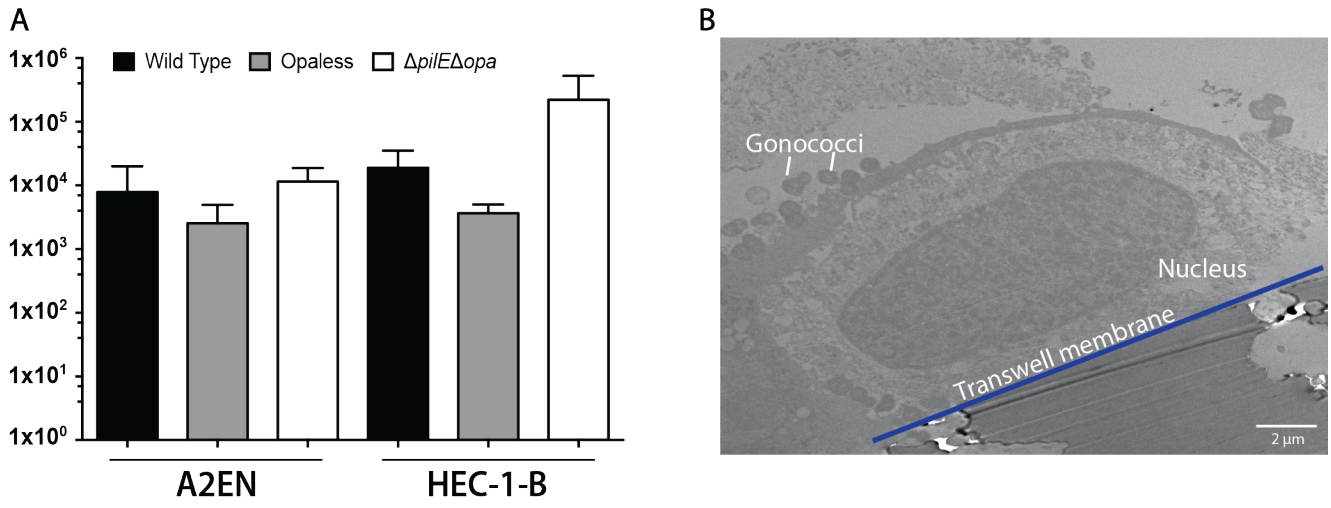

FIG 5 Infection of the 3D cervical cells (A2EN) by *N. gonorrhoeae* (Gc). Transmigration of Gc across the cervical epithelium model is similar to that obtained with a commonly used cell line (HEC-1-B) (A). TEM image of Gc attached to 3D cervical epithelial cells (B).

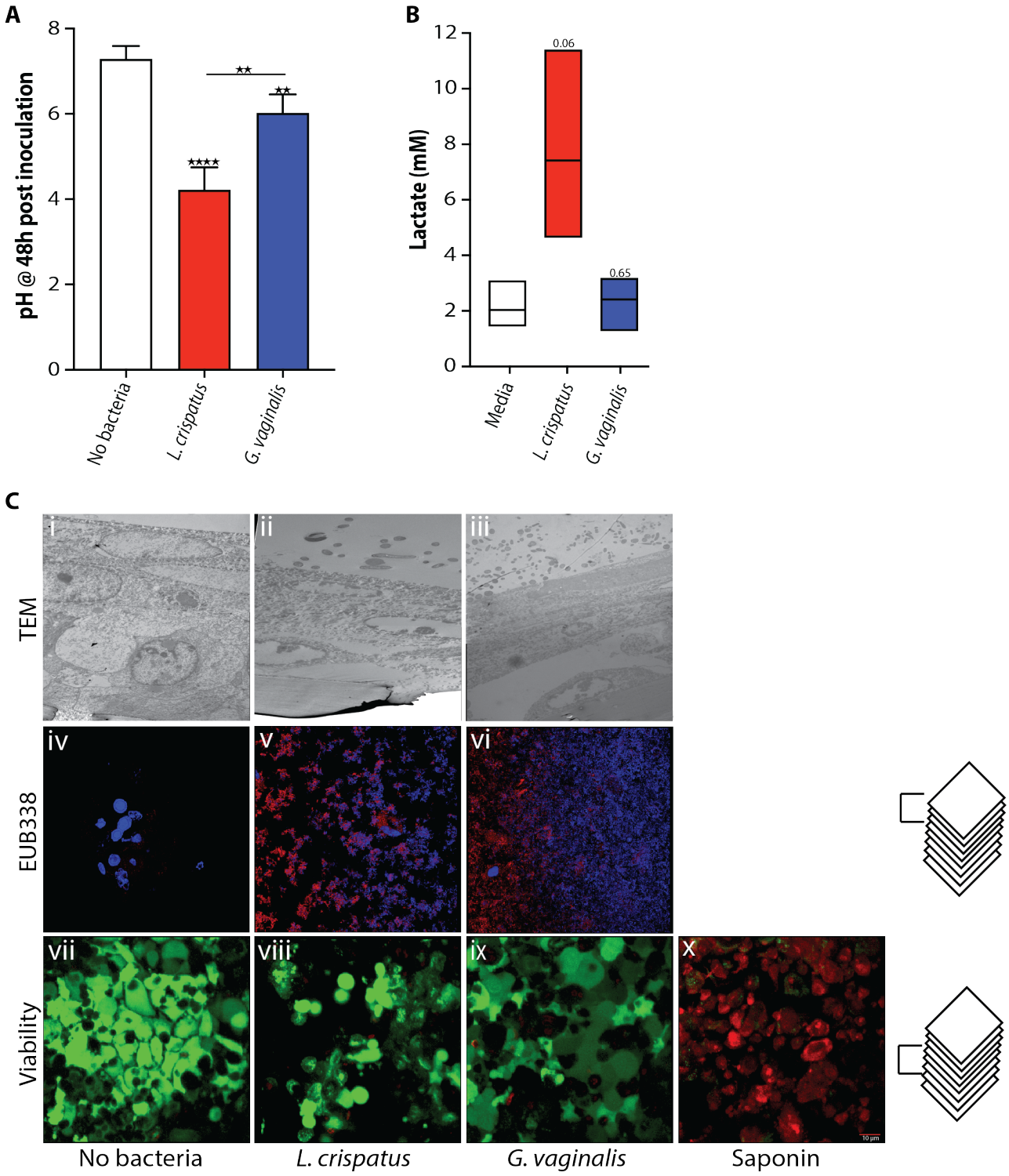

FIG 6 The 3D vaginal (VK2) epithelium model supports the growth of vaginal bacteria. pH (A) and D(-) lactate concentrations (B) of apical media after 48h of anaerobic bacterial growth on 3D VK2 cells. TEM, FISH and viability images of bacteria and host cells after 48h of growth (C).